

Rotating gliding arc assisted water splitting in atmospheric nitrogen

Hao Zhang^a, Fengsen Zhu^a, Xiaodong Li^{a,*}, Kefa Cen^a, Changming Du^b, Xin Tu^{c,*}

^a State Key Laboratory of Clean Energy Utilization, Zhejiang University, 38# Zheda Road, Hangzhou, Zhejiang 310027, China

^b School of Environmental Science and Engineering, Sun Yat-Sen University, 135# Xingang Xi Road, Guangzhou, Guangdong 510275, China

^c Department of Electrical Engineering and Electronics, University of Liverpool, Brownlow Hill, Liverpool L69 3GJ, UK

ABSTRACT

In this study, hydrogen production from water splitting in N₂ using an atmospheric pressure rotating gliding arc (RGA) plasma was investigated. The effect of input H₂O concentration and total flow rate on the performance of the plasma water splitting process (e.g., H₂ and O₂ yield, H₂ production rate, and energy yield of H₂) was investigated. N₂ showed a pronouncedly facilitating effect on the H₂O splitting and H₂ production process due to the reactions of the excited N₂ species (e.g., electronically excited metastable N₂(A)) with the H₂O molecules. The maximum H₂ production rate reached up to 41.3 $\mu\text{mol s}^{-1}$, which is much higher than that of other typical non-thermal plasmas (e.g., $\sim 0.2 \mu\text{mol s}^{-1}$ for a dielectric barrier discharge). Optical emission diagnostics has shown that in addition to the NO, N₂, and N₂⁺ that were observed in the pure N₂ spectra, strong OH and NH emission lines also appeared in the H₂O/N₂ spectra. OH radical is considered as a key intermediate species that could contribute to the formation of H₂, O₂, and H₂O₂. The increase of the H₂O concentration could lead to a continuous enhancement of the OH intensity. The rotational temperature of N₂⁺ dropped drastically from 2875 ± 125 to 1725 ± 25 K with the addition of 1% (mol/mol) H₂O into the N₂ plasma.

Keywords: Rotating gliding arc, water splitting, hydrogen production, optical emission spectroscopy (OES), reaction mechanisms

* Corresponding author. Tel.: +86-571-87952037 (X. D. Li); +44-1517944513 (X. Tu)
E-mail address: lixd@zju.edu.cn (X. D. Li); xin.tu@liv.ac.uk (X. Tu)

1. Introduction

Hydrogen has been regarded as one of the most important and promising future energy carriers that can power fuel cells to generate electricity with high efficiency because of its high energy density and almost nil emission. Hydrogen can be produced from a wide range sources, including natural gas, hydrocarbons, biomass, waste, and water. Currently, almost 80-85% of the world's total hydrogen is produced via steam methane reforming [1]. However, to eliminate the reliance on fossil fuels, the unlimited water source must be the ultimate choice for extracting large amounts of hydrogen for widespread energy use. Although water electrolysis has been a commercial and extensively used method to produce hydrogen, it only accounts for 0.1-0.2% of the world's hydrogen production at the moment due to the high cost [2]. Many researchers have long been exploring different new ways of producing hydrogen directly from water splitting, such as thermal, catalytic, and photocatalytic water decomposition [3-6]. However, the low water conversion, low hydrogen production rate, and low energy yield of hydrogen using these technologies restrict the potential scale-up of this process.

Non-thermal plasma technology provides an attractive alternative to the conventional catalytic route for fuel production at low temperatures. In non-thermal plasmas, the overall gas temperature can be as low as room temperature, while the electrons are highly energetic with a typical electron temperature of 1-10 eV, which is sufficient to break down most chemical bonds of molecules and produce highly reactive species: free radicals, excited atoms, ions, and molecules for the initiation and propagation of chemical reactions. The non-equilibrium character of such plasma could overcome thermodynamic barriers in chemical reactions and enable thermodynamically unfavorable reactions to occur at low temperatures. High reaction rate and fast attainment of steady state in plasma processes allows rapid start-up and shutdown of the process compared to other thermal processes, which significantly reduces the energy cost and offers a promising H₂ production route [7, 8]. It should be noted that, water vapor splitting in traditional thermal plasma needs a relatively high temperature of around 1000 K [9].

Plasma-assisted water splitting process could potentially produce 1000 times more hydrogen than the conventional electrolysis process with a same dimension of electrolyser due to its volumetric nature [10]. Various non-thermal plasmas have been used for hydrogen production from water splitting, such as pulsed corona discharges [11], micro-hollow cathode discharges [12], dielectric

barrier discharges (DBD) [10, 13], and flat gliding arc discharges [14-16], creating promising possibilities for further application. However, the H₂ production rate in these plasma processes is still quite low. For example, only 0.3 to 20.7 $\mu\text{mol s}^{-1}$ of hydrogen can be produced using gliding arc plasmas with knife-shaped electrodes [15], which might be resulted from the relatively low energy density and retention time of reactant in the plasma process. In addition, further study is needed to obtain insights into the reaction mechanisms of water splitting in plasma processes which are still poorly understood.

In this study, a direct current (DC) rotating gliding arc (RGA) plasma reactor co-driven by a magnetic field and tangential flow [17], has been developed for hydrogen production from water splitting at atmospheric pressure. Compared to the traditional gliding arc systems with knife-shaped electrodes, the RGA reactor can generate a synergetic effect resulting from the combination of swirling flow and Lorentz force, which can make the arc rotate rapidly and steadily without extinction (with a rotational speed of up to 100 rotations per second (rps)), creating a three-dimensional stable plasma area with the increased retention time of the reactant in plasma chemical reactions. In addition, in conventional gliding arc reactors, a relatively high flow rate is required to push the arc moving along the electrode and produce a relatively large plasma area for chemical reactions whilst not all the gas flow can pass the plasma region, which in turn results in a low conversion of reactants due to the decrease of retention time [7]. In contrast, in the RGA reactor, a relatively low flow rate can still maintain a large plasma area and a long arc length, both of which enhance the reaction performance in plasmas. This unique character of the RGA plasmas allows using a wide range of feed flow rate (e. g., approximately 0.05~40 L/min in our system), which is more suitable for the industry applications. It should be noted that, several kinds of three-dimensional RGA reactors have been developed by different authors to enhance the efficiency of the gliding arc reactor. Cormier et al. reported a magnetic blow out gliding arc reactor, in which a rotating magnetic field was applied to the ionized particles thanks to a magnet [18] [19]. Hnatiuc et al. presented that the using of a permanent magnet inside of the inner electrode could increase the rotating angle of the useful discharge from around $2\pi/3$ to over 2π , ensuring a better transfer of the generated species to the injected gas and, respectively to the target to treat [20]. Lee et al. reported a study of the partial oxidation of methane using an AC rotating gliding arc that driven by tangential flow [21]. Three modes of plasma operations with different dynamic behaviors and arc lengths can

be observed in their reactor, resulted from the difference in the input energy density.

In our previous work, the RGA plasma has shown to be a powerful transient plasma with a relatively high level of energy density, which is beneficial for chemical processes and high-productivity systems [17, 22, 23]. The RGA system was also shown to significantly improve the performance of plasma methane conversion process with a maximum methane conversion of 91.8% and a hydrogen selectivity of 80.7%, both of which are much higher than those using other non-thermal plasmas [17].

In this study, the RGA plasma reactor has been developed for the splitting of water into hydrogen. The effect of input H_2O concentration and total flow rate on the performance (e.g., H_2 and O_2 yield, H_2 production rate, and energy yield of H_2) of the plasma water splitting process has been investigated. Optical emission spectroscopy (OES) diagnostics has been used to give new insights into the formation of reactive species in the plasma chemical reactions. In addition, the possible dominant reactions in the plasma water splitting process have been discussed. A comparison of the water splitting process using different technologies has been carried out.

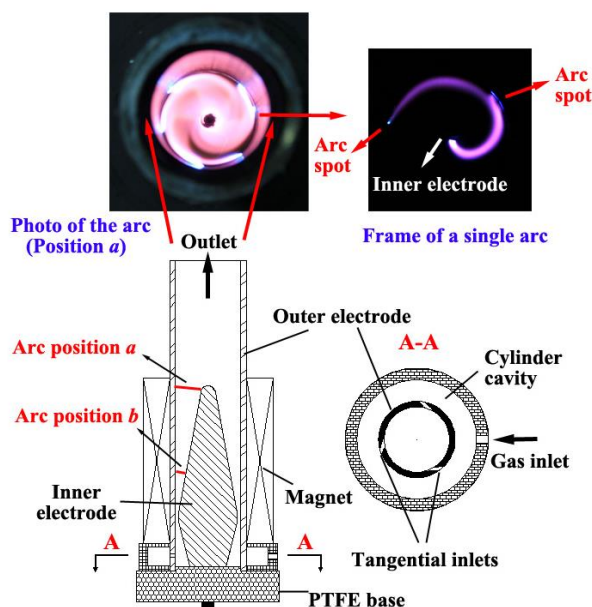


Fig. 1 Schematic diagram of the RGA reactor

(Total flow rate = 0.5 mol/min; input H_2O concentration = 10% (mol/mol).

High-speed camera: HG-100K with a CMOS sensor, exposure time: 997 μs)

2. Experimental setup and methods

2.1. RGA reactor

The configuration of the RGA reactor is shown in Fig. 1. A con-shaped stainless steel anode (100 mm in height) is placed inside of a stainless steel cylindrical cathode (inner diameter: 36 mm, height: 170 mm). The narrowest gap between the electrodes is 2 mm to facilitate the initial ignition of the arc. A magnet was placed outside the cathode to generate a magnetic field with a flux density of around 2000 G for the stabilization and acceleration of the arc. N₂ was used as a carrier gas and was injected through three tangential inlets (1 mm in diameter) at the bottom of the reactor to form a swirling flow in the reactor.

Typical photo image of the RGA discharge and the frame of a single arc recorded by a high-speed camera are also shown in Fig. 1. The arc was initially formed at the narrowest gap point between the electrodes and then propelled by the swirling flow and accelerated by the Lorentz force generated by the magnetic field. Finally, the arc would be anchored at the position *a* or *b* (depends on the total feed flow rate) of the anode, and rotated rapidly and steadily without extinction, forming a stable plasma volume for chemical reactions. The rotation speed of the arc was around 75 rps in this case, while the rotating arc is quite long (position *a*), with a length of approximately 46.5 mm, estimated from the frames of the arc. One or two cathode spots could be observed between the arc column and the cathode, and the cathode spots moved along the inner wall of the outer electrode with a speed of around 8.5 m/s.

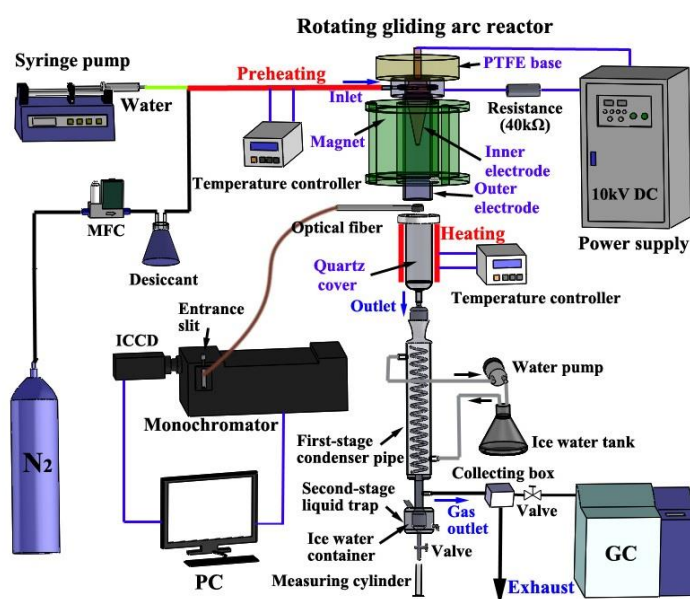


Fig. 2 Schematic diagram of the RGA plasma-assisted water splitting system

2.2. Experimental setup and gas analysis

Fig. 2 shows the schematic diagram of the experimental setup. The flow rate of the inlet N₂ was controlled by a MFC (Sevenstar D07-series), and a silica gel desiccant was added after the MFC to remove moisture in the gas. Water was controlled and injected into the gas tube using a high-resolution syringe pump (Harvard, 11 plus). In this way, the total feed flow rate (0.1-0.7 mol/min) of the mixed stream and the input H₂O concentration (1-30 % (mol/mol)) could be controlled. The mixed stream was then heated to 120°C in a stainless steel pipe with an inner diameter of 4 mm (40 cm in length) equipped with a temperature controller system, to generate a steady-state vapor before flowing into the RGA reactor. The quartz cover of the reactor was also heated to 120°C to prevent vapor condensation on the inner wall. The plasma reactor was connected to a DC power supply (380 V/10 kV) with a 40-kΩ resistance connected in the circuit to limit and stabilize the breakdown current. A two-stage condenser was placed at the exit of the plasma reactor to condense and collect the condensable vapors in the effluent consisting of a first-stage condenser pipe equipped with an ice water cycle system and a second-stage liquid trap placed inside of an ice water container.

The gaseous products (H₂ and O₂) were measured by a gas chromatograph (GC) (GC9790A, Fuli Analytical Instrument) equipped with a thermal conductivity detector (TCD). The emission spectra of the plasmas were recorded by a 750-mm monochromator (PI-Acton 2750, grating: 1800 grooves/mm) equipped with an intensified charge-coupled device (ICCD, PI-MAX 2, 512×512 pixel). An optical fiber was placed at the exit of the RGA reactor to collect the plasma radiation.

2.3. Definition of parameters

The effect of input H₂O concentration and total flow rate on the performance of water splitting process in the RGA reactor was investigated in terms of H₂ yield $Y(H_2)$, H₂ production rate $P(H_2)$, O₂ yield $Y(O_2)$, H₂/O₂ molar ratio, and energy yield of H₂ EY .

Hydrogen yield is defined as,

$$Y(H_2)(\%) = \frac{\text{moles of H}_2 \text{ produced}}{\text{moles of H}_2\text{O introduced}} \times 100\% \quad (1)$$

Hydrogen production rate is defined as,

$$P(H_2)(\text{mmols}^{-1}) = \text{mmoles of } H_2 \text{ produced per second} \quad (2)$$

Oxygen yield is defined as,

$$Y(O_2)(\%) = \frac{2 \times \text{moles of } O_2 \text{ produced}}{\text{moles of } H_2O \text{ introduced}} \times 100\% \quad (3)$$

The energy yield of H_2 is defined as,

$$EY(\text{g/kWh}) = \frac{\text{grams of } H_2 \text{ produced per hour}}{\text{Discharge power (kW)}} \quad (4)$$

The specific energy input (*SEI*) is defined as

$$SEI(\text{kJ/mol}) = \frac{\text{Discharge power (kW)} \times 60}{\text{Total molar flow rate (mol/min)}} \quad (5)$$

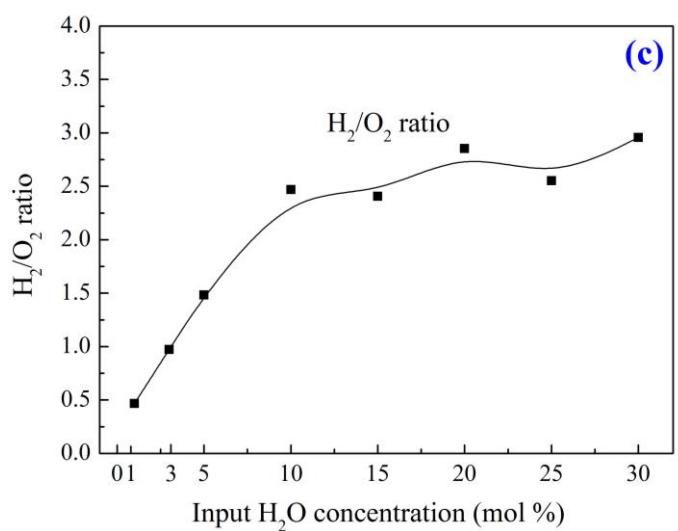
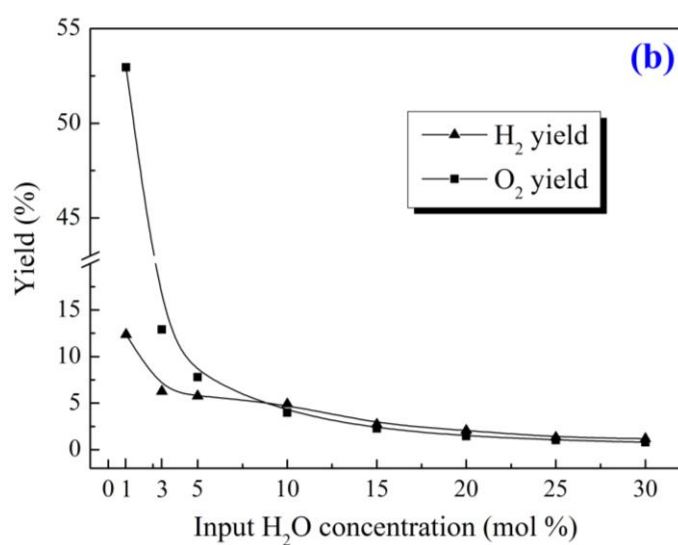
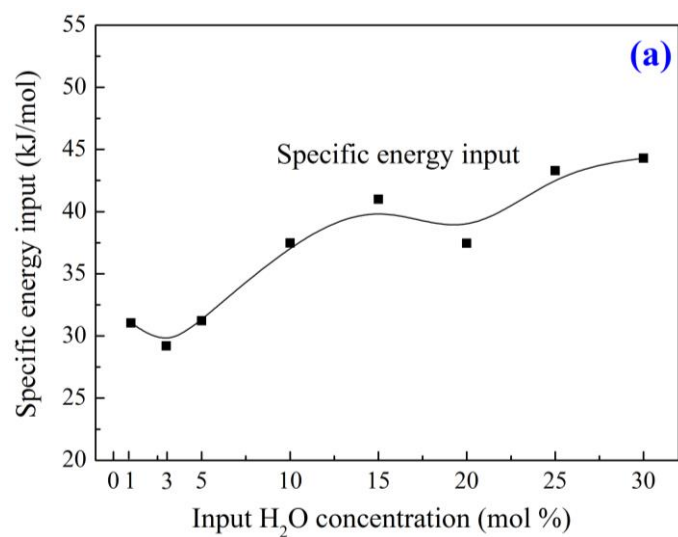
3. Results and discussion

3.1. RGA assisted water splitting for hydrogen production

3.1.1. Effect of input H_2O concentration

Fig. 3 shows the effect of input H_2O concentration on the specific energy input, H_2 and O_2 yield, H_2/O_2 ratio, H_2 production rate, and energy yield of H_2 . It is considered that the excited N_2 species (e.g., electronically excited metastable $N_2(A)$ and vibrationally excited $N_2(X, v)$) that formed in the plasma probably substantially contribute to the dissociation of H_2O molecules, particularly at a low concentration of H_2O (e.g., 1-5% (mol/mol), see Section 3.2). Therefore increasing the H_2O concentration from 1 to 5% (mol/mol) (decreasing the N_2 concentration from 99 to 95% (mol/mol)) leads to a significant decrease in both the H_2 and O_2 yield, from 12.4 to 5.8% and from 53.0 to 7.8%, respectively.

With a further increase of H_2O concentration, both the H_2 and O_2 yield drop slightly, even though the specific energy input increases. Similar results were also obtained in other works [24]. It is interesting to note that the facilitating effect of N_2 on the decomposition of reactants in plasmas (e.g., methane, methanol, and ethylene) has been widely reported [17, 23, 25-27].



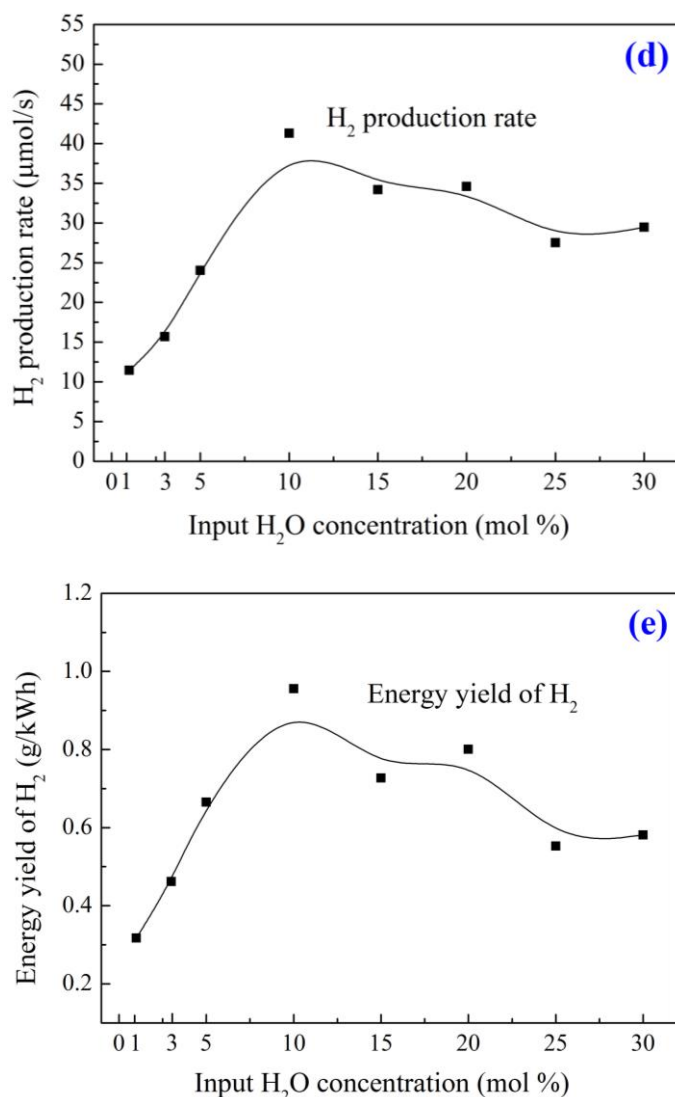


Fig. 3 Effect of input H₂O concentration on (a) specific energy input, (b) H₂ and O₂ yield, (c) H₂/O₂ ratio, (d) H₂ production rate, and (e) energy yield of H₂ (flow rate = 0.5 mol/min)

From the stoichiometry of the H₂O splitting reaction, a H₂/O₂ ratio of 2.0 could be expected, whereas in this study the H₂/O₂ ratio at a H₂O concentration of 1% (mol/mol) is only 0.47, as shown in Fig. 3(c). This might be attributed to the formation of a larger amount of NH radicals at a low H₂O concentration (see Eqs. (17)-(21)), which probably then further react with H or H₂ to produce NH₃ (see Eq. (22)). In agreement with these results, a maximum NH emission intensity reached at a H₂O concentration of 1% (mol/mol), and with a further increase in the H₂O concentration, the NH intensity decreased continuously (see Fig. 7), contributing to a further enhancement in the H₂/O₂ ratio.

A H₂/O₂ ratio of between 2.4 and 2.9 is obtained with a H₂O concentration of 10 to 30%

(mol/mol), which is higher than the stoichiometric H₂/O₂ ratio of the overall reaction. This is probably resulted from the increased production of some O-containing species (e.g., H₂O₂, O₃, NO) (see Section 3.2), with the increase of the H₂O concentration.

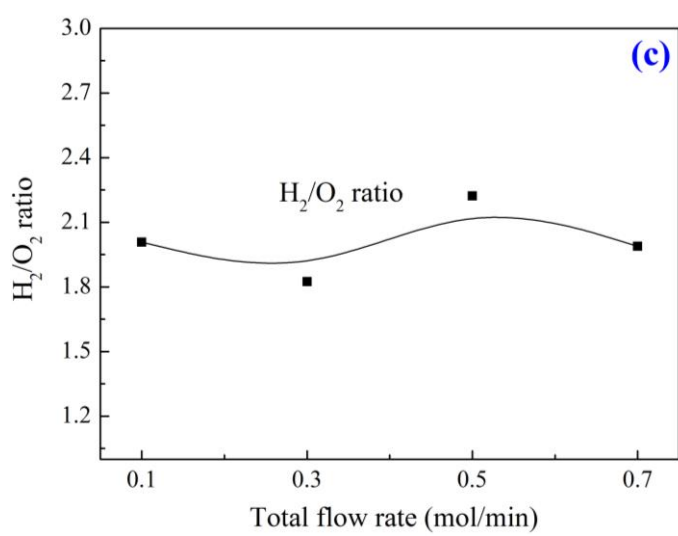
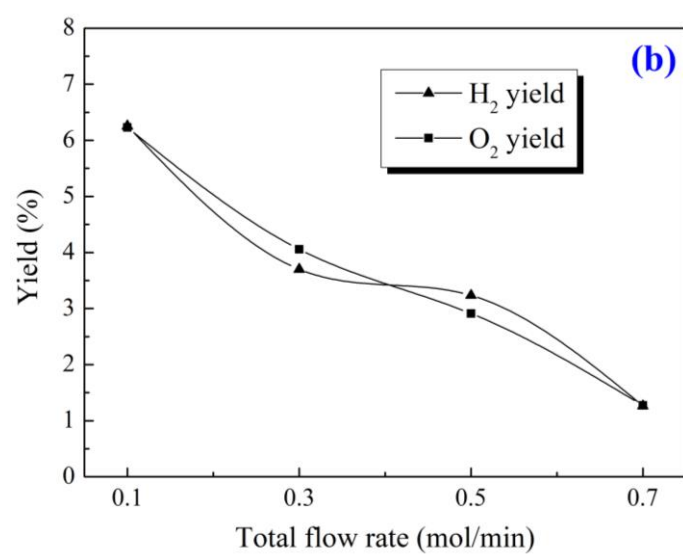
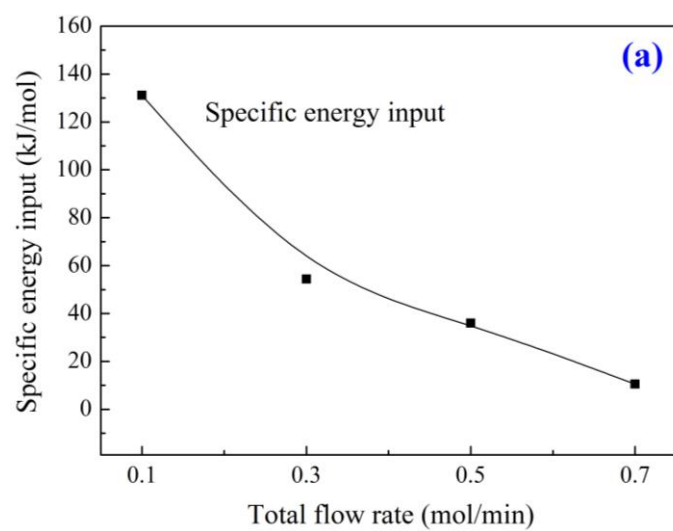
The hydrogen production rate and energy yield of H₂ show similar evolution with increasing the H₂O concentration: initially increase as the H₂O concentration passes from 1 to 10% (mol/mol), and then declines with a further increase of the H₂O concentration, as shown in Fig. 3(d) and (e). The maximum hydrogen production rate and energy yield of H₂ are 41.3 μmols^{-1} and 0.96 g kWh⁻¹, respectively at a H₂O concentration of 10% (mol/mol) and in this case, the H₂ and O₂ yield are 4.9 and 4.0%, respectively.

3.1.2. Effect of total flow rate

The effect of total flow rate on the specific energy input, H₂ and O₂ yield, H₂/O₂ ratio, H₂ production rate, and energy yield of H₂ is shown in Fig. 4. Based on the OES analysis (see Section 3.3.2 and 3.4), the emission intensities of different species, together with the rotational temperature of the plasma all vary slightly with the increase of flow rate (except 0.7 mol/min due to the difference in arc rotation mode), indicating that the characteristics of the H₂O/N₂ plasma seems to be relatively independent of the flow rate. Therefore, it is supposed that the increased residence time with increasing flow rate could substantially contribute to the decrease in the H₂ and O₂ yield. The estimated residence time, determined as the volume of the plasma zones divided by the volumetric gas flow rate, drops drastically from 1.6 to 0.3 ms with the increase of total flow rate from 0.1 to 0.7 mol/min. The specific energy input decreases almost linearly with the increase of flow rate, which could also lead to a decrease in both the H₂ and O₂ yield, as shown in Fig. 4(a) and (b).

The H₂/O₂ ratio varies slightly from 2.0 to 2.2 with rising flow rate. The maximum H₂ production rate is obtained at a flow rate of 0.5 mol/min. The remarkable decrease of the production rate with increasing flow rate from 0.5 to 0.7 mol/min arose from the significant decrease in the discharge power from 301.0 to 123.2 W, resulted from the change of the arc rotation mode (as discussed in Section 3.3.2). The energy yield of H₂ escalates with the increase of flow rate.

According to the experimental results, an input H₂O concentration of 10% (mol/mol) and a total flow rate of approximately 0.5 mol/min should be recommended for a relatively high H₂ yield and H₂ production, as well as a high energy yield of H₂ in the RGA N₂ plasmas.



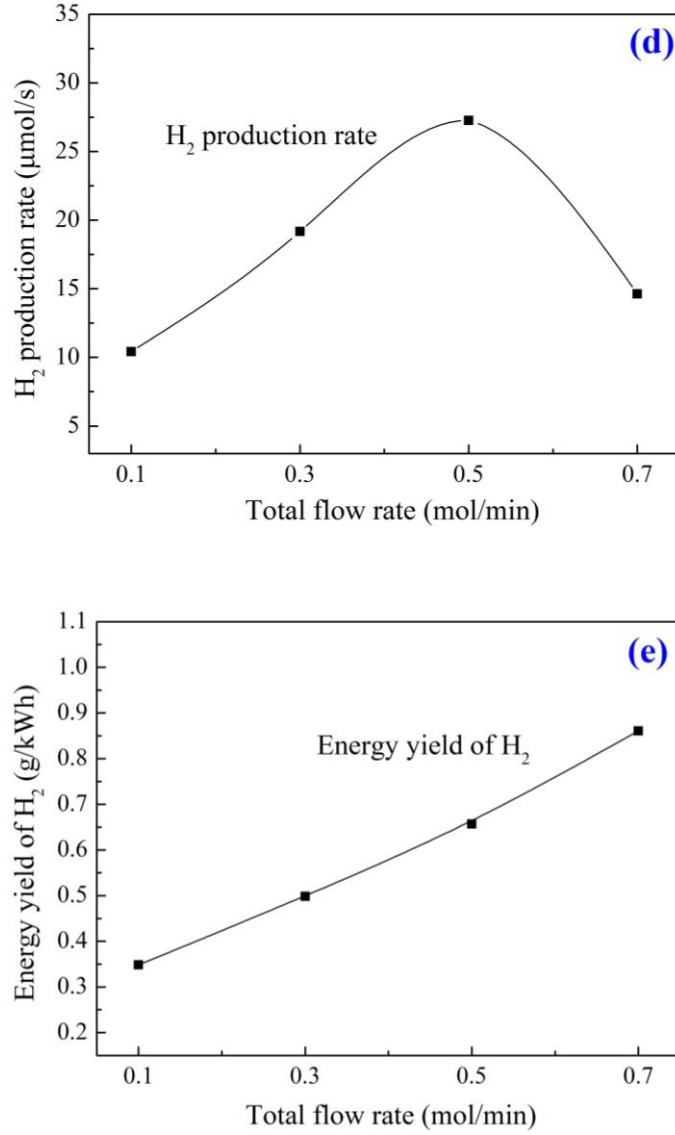


Fig. 4 Effect of total flow rate on (a) specific energy input, (b) H₂ and O₂ yield, (c) H₂/O₂ ratio, (d) H₂ production rate, and (e) energy yield of H₂ (H₂O concentration = 10% (mol/mol))

3.2. Optical diagnostics and reaction mechanisms of the plasma chemical processes

Optical emission diagnostics was carried out to understand the formation of reactive species and to give new insights into the possible reaction mechanisms of the plasma water splitting processes. Typical emission spectra of the pure N₂, 5% (mol/mol) H₂O/N₂, and 15% (mol/mol) H₂O/N₂ plasmas are shown in Fig. 5. The spectra of the pure N₂ RGA are clearly dominated by the N₂ second positive band system (SPS) ($C^3\Pi_u(v') \rightarrow B^3\Pi_g(v'')$, $\Delta v=2,1,0,-1,-2,-3$) and the N₂⁺ first negative band system (FNS) ($B^2\Sigma_u^+(v') \rightarrow X^2\Sigma_g^+(v'')$, $\Delta v=-1$).

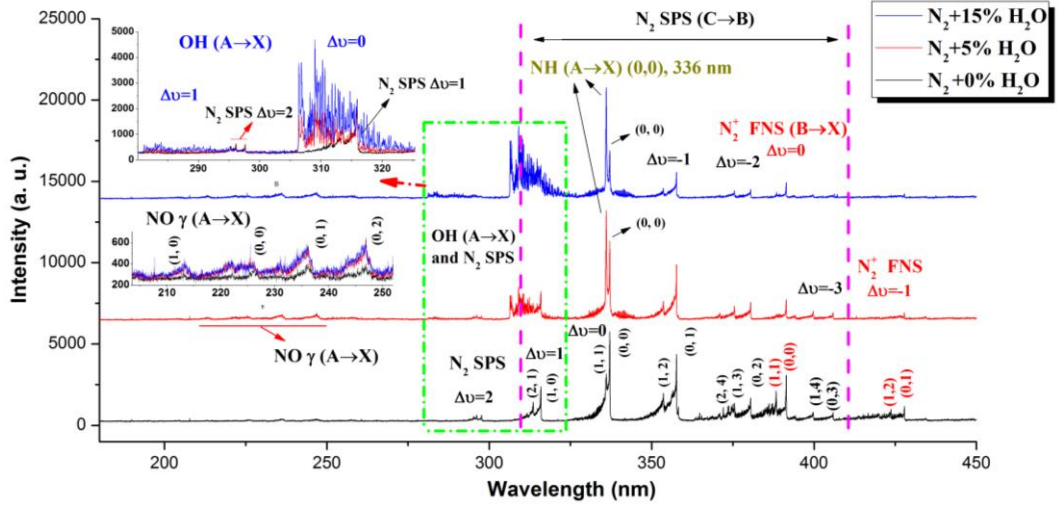
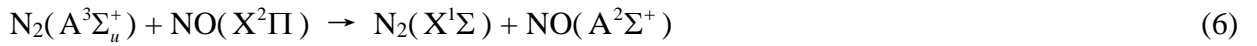


Fig. 5 Emission spectra of pure N₂, 5% (mol/mol) H₂O/N₂, and 15% (mol/mol) H₂O/N₂ plasmas (flow rate = 0.5 mol/min)

Similar with other works [28, 29], although the N₂ gas used is 99.99% in purity, several weak NO γ ($A^2\Sigma^+(v') \rightarrow X^2\Pi(v'')$) bands with vibrational sequences of $\Delta v=1,0,-1,-2$ (200-250 nm) also appear in the pure N₂ spectra, indicating the existence of NO($A^2\Sigma^+$) radicals in plasmas. The NO γ band emission, which is due to the existence of trace oxygen in the system, is a spectral signature of the presence of the metastable state N₂($A^3\Sigma_u^+$), and the concentration of the NO($A^2\Sigma^+$) radicals depends on that of the N₂($A^3\Sigma_u^+$) radicals, since the NO($A^2\Sigma^+$) radicals in the plasma bulk mainly produce from the reaction of N₂($A^3\Sigma_u^+$) and NO($X^2\Pi$) through [28]:



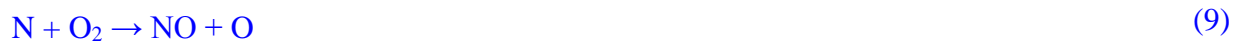
The ground state NO($X^2\Pi$) is produced mainly via the following reaction:



For the 5% H₂O/N₂ and 15% H₂O/N₂ plasmas, in addition to the N₂ SPS bands, N₂⁺ FNS bands, and NO γ bands that are observed in the pure N₂ spectra, the OH ($A^2\Sigma^+(v') \rightarrow X^2\Pi(v'')$, $\Delta v=1,0$) system in 280-325 nm and the strong NH ($A^3\Pi(v') \rightarrow X^3\Sigma(v'')$) (0, 0) transition centered at 336.0 nm also appear in the spectra. The OH and NH spectral lines become more and more predominant in the spectra with increasing H₂O concentration. The OH(A→X) transitions of $\Delta v=0$ are partly overlaid by

the N₂ SPS transitions of $\Delta v=1$ in 311-316 nm, as shown in the enlarged spectra of OH in Fig. 3.

In the H₂O/N₂ plasmas, NO can also form from the reaction of N atoms with the produced OH radicals or O₂ molecules through the reactions [30],



And then, NO₂ could form from the combination of NO and O [14, 24],



The formation of OH radicals (i.e., the dissociation of H₂O molecules) could take place from four possible channels in the atmospheric H₂O/N₂ plasmas. The first one is from the electron impact dissociation of water molecules [31-33],



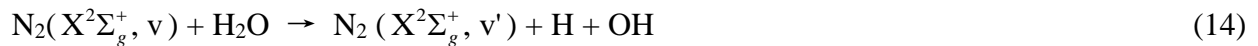
Some authors also reported the formation of OH from the electron dissociative recombination of H₂O⁺ or H₃O⁺ ions (Eq. (12)), which are generated by charge transfer from primary ions (e.g., N₂⁺) to H₂O molecules or from electron ionization of H₂O molecules [34-36].



This channel is supposed to be non-ignorable in the RGA plasmas, considering the population of N₂⁺ ions in the plasma bulk, which could transfer charge to the H₂O molecules to produce H₂O⁺. In addition, the ionization energy of H₂O (15.1 eV) is within the range of the ionization potential of N₂ (15.58 eV). Excited N₂⁺ is observed in the spectra, indicating that H₂O⁺ ions could be formed from direct electron ionization of H₂O [36]. Bruggeman et al. demonstrated that the electron dissociative recombination reaction is clearly an important reaction in gas-water plasma with an electron energy of 1-2 eV, because the cross-section for OH(A) production by electron dissociative recombination of H₂O⁺ or H₃O⁺ is about four orders of magnitude larger than the maximum cross-section for electron dissociative excitation of H₂O [35].

In addition, in the H₂O/N₂ RGA plasmas, initially formed highly energetic electrons can interact with N₂ molecules to produce a cascade of processes yielding a variety of chemically reactive

species (e.g., electronically excited metastable $N_2(A^3\Sigma_u^+)$ and vibrationally excited $N_2(X^2\Sigma_g^+, v)$) [26, 37, 38]. These species are believed to substantially contribute to the splitting of H_2O molecules via Eqs. (13)-(14), particularly at a low concentration of H_2O (e.g., 1-5% (mol/mol)) [24, 39].



The reaction rate of Eq. (13) is shown to be one order of magnitude lower than that of the electron impact H_2O dissociation reaction (Eq. (11)), in case of the mean electron energy of 3.3 eV and gas temperature of 300 K [40].

The vibrational temperature of the RGA N_2 plasmas was shown to be in the range of 4800-5100 K according to our previous study [17]. The vibrationally excited $N_2(X, v < 12)$ with relatively low excitation energy (< 3.23 eV) are probably abundant in the plasma bulk. By solving the Boltzmann equation using the BOLSIG+ software (a commonly used Boltzmann equation solver [41]), the rate coefficients for the production of $N_2(X, v=1-12)$ excited species are in the range of 10^{-9} - 10^{-27} cm^3s^{-1} .

Our previous study of RGA plasma methanol decomposition process also showed that the vibrationally and electronically excited N_2 species (e.g., $N_2(A)$ and $N_2(X, v)$) probably played a critical role in the conversion of methanol, leading to a higher methanol conversion in the CH_3OH/N_2 plasmas compared to the CH_3OH/Ar plasmas due to the presence of more reaction pathways [23]. Aerts et al. demonstrated that the quenching reactions with metastable $N_2(A)$ appear to be important, while the direct electron impact dissociation reactions are negligible in the destruction of ethylene (10-10,000 ppm) using a DBD air plasma [27]. In addition, Damiy et al. and Pintassilgo et al. have shown that the excited N_2 species ($N_2(A)$ and $N_2(X, v)$) are critical in the initial decomposition of methane in 2-44.4% (v/v) CH_4/N_2 glow plasmas [26, 37, 38, 42].

In addition, O_2 (which can then produce O atoms) concentration could affect OH generation through the following reactions [24, 31, 33, 43],

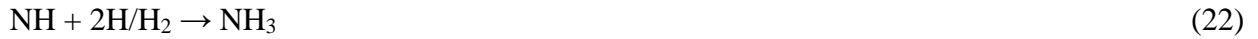


It should be noted that, the production of OH by thermal dissociation for the relative low gas temperatures (< 2000 K in this study, see Section 3.3) is clearly negligible in this study [35].

NH radicals were produced from the reactions of N atoms that formed from electron impact dissociation of N₂, with H atoms, H₂, and H₂O molecules or OH radicals via the following reactions [30, 44, 45],



NH₃ is probably formed through the coupling reactions of NH with H or H₂ (Eq. (22)) [46].



The main gaseous products of the water splitting process: H₂ and O₂ are not observed in the spectra, but can be generated via the following reactions [10, 24, 30, 39],



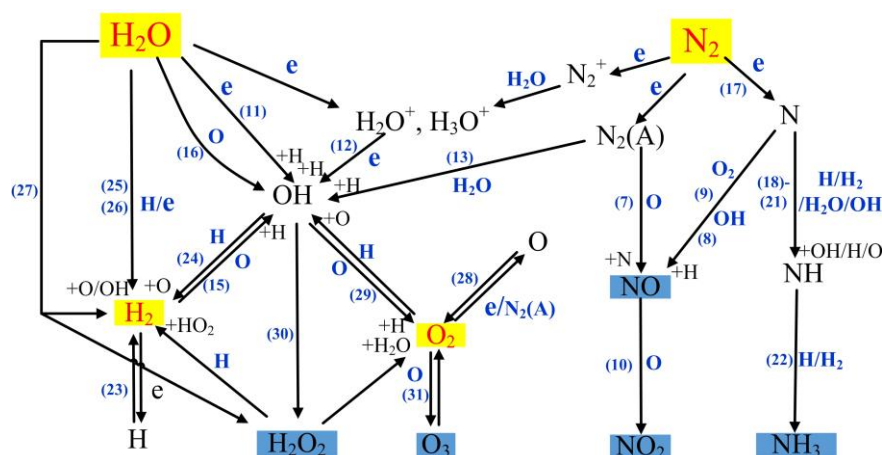
Eqs. (23)-(25), (28), and (29) probably play a important role in the formation of H₂ and O₂ due to the abundance of H, O, OH, and H₂O species in the plasma bulk.

In addition, as evidenced by many researchers in gas-liquid gliding arc plasmas [14, 16, 47, 48], H₂O₂ and O₃ could probably produce as intermediate products in the H₂O/N₂ RGA plasmas. H₂O₂ is generated mainly from the combination of two OH radicals (Eq. (30)) or two H₂O molecules (Eq. (27)), and O₃ forms primarily from the reaction of O₂ molecules with O atoms (Eq. (31)) [10, 30, 49]. It should be noted that, both H₂O₂ and O₃ could be readily dissociated by thermal effect in the process considering the high gas temperature in the H₂O/N₂ RGA plasmas (1400-1825 K, see Section

3.4).



The most probable dominant reaction pathways in the RGA water splitting processes in N_2 are schematically shown in Fig. 6. We can see OH radical is shown to be a key intermediate species that could contribute to the formation of H_2 , H_2O_2 , and O_2 .



The numbers that labeled on the reaction path denote the corresponding numbered reactions in this paper

Fig. 6 Schematic representation of the mechanisms of water splitting in N_2 RGA plasmas

3.3. Effects of input H_2O concentration and total flow rate on the emission intensities of observed species

3.3.1. Effect of input H_2O concentration

In order to obtain better insights into the mechanisms of the plasma chemical reactions, the emission lines of the $\text{OH}(\text{A} \rightarrow \text{X})$ (0, 0) transition at 309.0 nm, $\text{NH}(\text{A} \rightarrow \text{X})$ (0, 0) transition at 336.0 nm, N_2 SPS (0, 0) transition at 337.1 nm, and N_2^+ FNS (0, 0) transition at 391.4 nm were selected to investigate the effects of input H_2O concentration (Fig. 7) and total flow rate (Fig. 8) on the emission intensities of these species.

Fig. 7 shows the addition of 1% (mol/mol) H_2O into N_2 plasma leads to the formation of OH and NH, as well as a noticeable increase of N_2 intensity and a drastic drop of N_2^+ intensity. Then, when further increasing the H_2O concentration, the OH intensity continues to increase, whereas the NH, N_2 and N_2^+ intensity decrease.

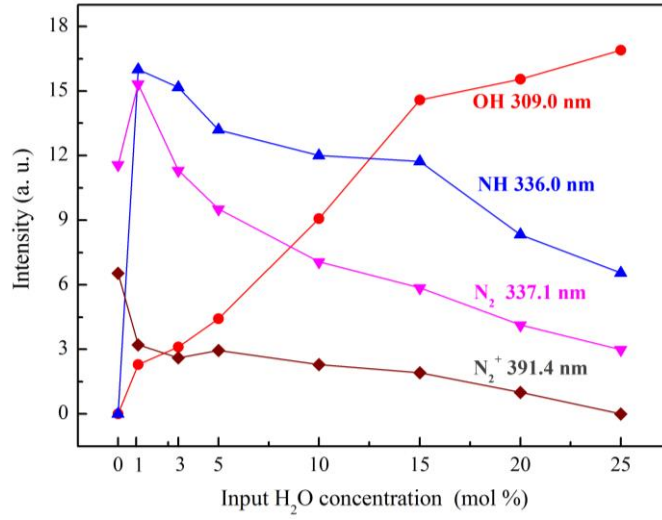


Fig. 7 OH, NH, N₂, and N₂⁺ emission intensities as a function of input H₂O concentration (flow rate = 0.5 mol/min)

In agreement with other works [32, 43], increasing amount of H₂O addition leads a continuously remarkable increase in the OH intensity. In the H₂O/N₂ plasmas, in addition to the direct electron impact dissociation of H₂O (Eq. (11)), as well as dissociative electron recombination of H₂O⁺ (H₃O⁺) (Eq. (12)), the reactions of excited N₂ species (e.g., electronically excited N₂(A)) with H₂O molecules (Eq. (13)) are also considered to play an important role in the generation of OH radicals, which can be evidenced by the following two aspects. Firstly, the N₂(A) molecules are abundant in the plasma bulk, inferring from the high intensity of the N₂ SPS transitions (see Fig. 5), and therefore the collision probability between the introduced H₂O molecules and excited N₂(A) molecules should be quite high. Secondly, as shown in Fig. 7, the N₂ intensity exhibits a relatively faster decrease rate compared to other species (e.g., N₂⁺ and NH) with the increase of H₂O concentration, indicating efficient energy transfers from the excited N₂ species to H₂O molecules.

Due to the quenching effect of H₂O molecules on the plasma system, the mean electron energy (or electron temperature) is considered to decrease with the increase of H₂O concentration [50], giving rise to a decrease in all the NH, N₂, and N₂⁺ emission intensities. In addition, the estimated gas temperature slightly declined from 1725 ± 125 to 1400 ± 75 K (See Section 3.4), whereas the discharge power rose from 261.7 to 361.0 W with an increase of the H₂O concentration from 1 to 25% (mol/mol). Therefore, the electron density in the plasma bulk is expected to increase with rising H₂O

concentration due to the increased discharge power, which could also lead to an enhancement in the OH emission intensity.

With the addition of 1% (mol/mol) H₂O into N₂, a noticeable increase of N₂ intensity appears, probably resulted from the increase of electron density. Whereas, as the H₂O concentration further increases, the N₂ intensity then drops with a relatively fast rate, which should arise from the decrease of electron temperature and the increased energy transfers to the H₂O molecules, as discussed above.

The addition of 1% (mol/mol) H₂O into N₂ leads to a significant drop of the N₂⁺ intensity, and a further increase of H₂O concentration results in a slight decrease of the N₂⁺ intensity. Finally, no N₂⁺ spectral line appears in the spectra at a H₂O concentration of 25% (mol/mol). Due to the high ionization energy of N₂ (15.58 eV) [36], the N₂⁺ emission intensity is very sensitive to the electron temperature, and thus the decrease of electron temperature with increasing H₂O concentration should substantially contribute to the decrease of the N₂⁺ intensity.

For the NH emission, the addition of 1% (mol/mol) H₂O into N₂ drastically increases the NH intensity, resulted from the introduction of the H-containing species (e.g., H₂O, H₂, OH, and/or H) into the plasma system that can react with N atoms to produce NH via Eqs. (17)-(21). Then, the decrease of electron temperature and/or the reduce of H or H₂ concentration could contribute to the decrease of NH intensity with a further increase of the H₂O concentration.

3.3.2. Effect of total flow rate

Fig. 8 shows that the emission intensities of OH, NH, N₂, and N₂⁺ appear to be weakly dependent on the flow rate with a flow rate of 0.1-0.5 mol/min. This is because, the N₂/H₂O plasma system with only 10% (mol/mol) H₂O is full of excited N₂ molecules and N₂⁺ ions, therefore their concentrations can hardly be affected by increasing flow rate. The slight increase of NH or OH emission intensity probably arises from the increase of electron density with increasing flow rate.

It is interesting to note that, increasing flow rate from 0.5 to 0.7 mol/min can drastically decrease all the emission intensities of NH, OH, N₂, and N₂⁺, which is due to the change of the arc rotation mode. When the flow rate was gradually increased to 0.7 mol/min, the rotating arc suddenly shifted from position *a* to *b*, as shown in Fig. 1. A reasonable explanation of this phenomenon was proposed in our previous work [51]. A longer distance between the plasma disc at point *b* results in the pronounced drop of the emission intensities. In addition, the drastic decrease of discharge power

from 301.0 to 123.2 W with increasing flow rate from 0.5 to 0.7 mol/min could also contribute to the noticeable decrease of the emission intensities of these species.

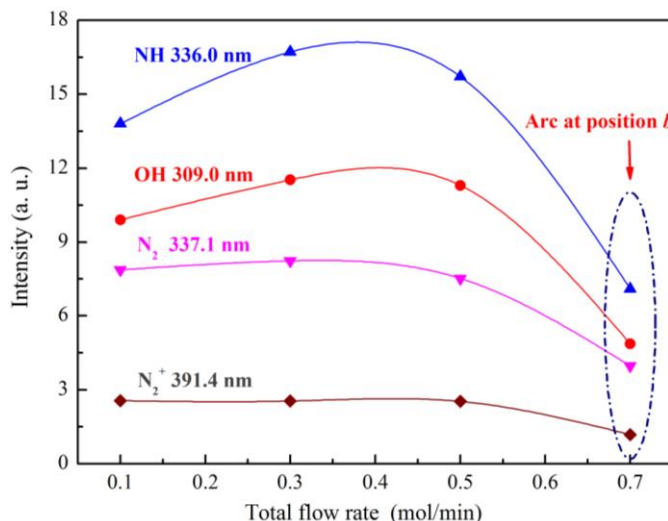


Fig. 8 OH, NH, N₂, and N₂⁺ emission intensities as a function of total flow rate
(H₂O concentration = 10% (mol/mol))

3.4 Determination of the rotational temperatures

The N₂⁺(B→X) (0, 0) transition in 380-392 nm were selected for rotational temperature determination, based on finding the best fit between experimental and simulated spectra using Lifbase software [52], which is commonly used in atmospheric pressure plasmas [50]. The rotation-translation relaxation of N₂⁺(B) is sufficiently fast to equilibrate the rotational temperature and the gas kinetic temperature before the rotationally excited N₂⁺(B) molecules undergo radiative decay, therefore the rotational temperature of N₂⁺(B) is considered approximately equally to the gas temperature in atmospheric pressure plasma [53].

The effects of input H₂O concentration and total flow rate on the rotational temperatures of the RGA plasmas are shown in Fig. 9 and Fig. 10 respectively. It is interesting to note that a comparison of Fig. 9 and Fig. 7 shows the rotational temperature of N₂⁺ follows a similar evolution of the emission intensity of N₂⁺ with the increase of the H₂O concentration. The addition of 1% H₂O (mol/mol) into the system leads to a drastic drop of the rotational temperature from 2875 ± 125 to 1725 ± 25 K, resulted from the strong cooling effect of H₂O molecules that have large heat capacities. The slight elevation of gas temperature from the H₂O concentration of 1 to 5% (mol/mol) probably

comes from the extremely rapid vibration-translation (V-T) relaxation of H₂O molecules [54]. Then, with increasing amount of H₂O addition, the rotational temperature continues to decrease.

As shown in Fig. 10, the rotational temperature of N₂⁺ first decreases slowly as the flow rate passes from 0.1 to 0.5 mol/min, and then drops drastically from 1600 ± 25 to 1075 ± 75 K with a further increase of flow rate to 0.7 mol/min. A similar evolution of the emission intensity of N₂⁺ was also observed with increasing flow rate, as shown in Fig. 8. The increased heat loss in the plasma system at a higher flow rate could make a significant contribution to the decrease of the rotational temperature of N₂⁺. The noticeable drop of the rotational temperature from 1600 ± 25 to 1075 ± 75 K as the flow rate passes from 0.5 to 0.7 mol/min should be ascribed to the drastic decrease of the discharge power from 301.0 to 123.2 W when the arc position shifts from *a* to *b*, as mentioned in Section 3.3.2.

Note that the rotational temperatures determined by the N₂(C→B) spectral lines in flat gliding arc N₂ plasmas are 1000-1500 K, which is slightly lower than the RGA H₂O/N₂ plasmas in this study [55]. In addition, in an alternate current (AC) rotating gliding arc H₂O/Air plasma driven by tangential flow (discharge power = 44 W, total flow rate = 4.0 L/min, water vapour = 0.63 % (v/v)), the rotational temperatures derived from N₂(C→B) and N₂⁺(B→X) are 2000-2500 K [56].

In addition, our previous study have shown that the mean electron temperature and electron density of the RGA N₂ plasma were 0.8-0.9 eV and $1.5-4.9 \times 10^{13} \text{ cm}^{-3}$, respectively [17].

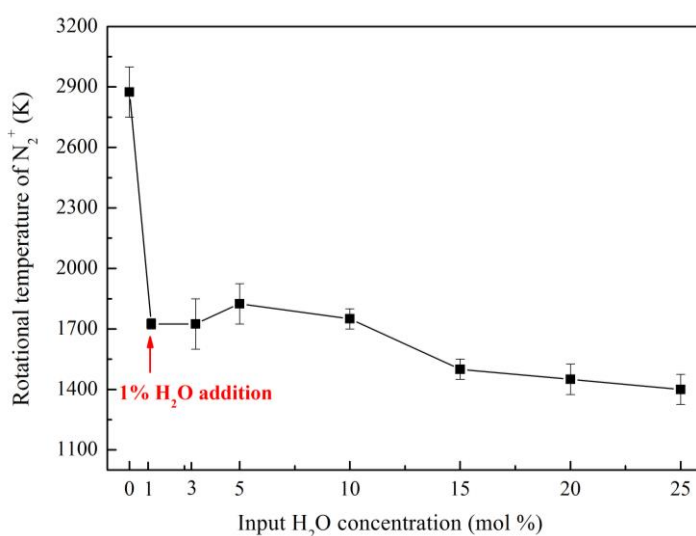


Fig. 9 Rotational temperatures of N₂⁺ as a function of input H₂O concentration
(flow rate = 0.5 mol/min)

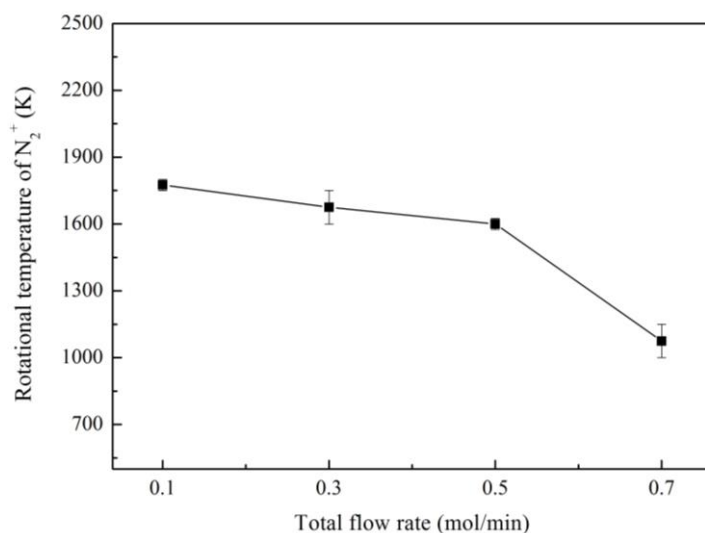


Fig. 10 Rotational temperatures of N_2^+ as a function of total flow rate
(H_2O concentration = 10% (mol/mol))

3.5. Comparison of different technologies for hydrogen production from water splitting

Table 1 shows a comparison of the performance (e.g., H_2 yield, H_2 production rate, and energy yield of H_2) of water splitting for hydrogen production using electrolysis, photocatalysis, and typical non-thermal plasma systems.

With the advantages of high volumetric productivity, fast ignition, as well as low investment and operating costs, various plasma reactors have been investigated by many researchers for hydrogen production from water splitting, whereas the H_2 yield is still unsatisfactory, only 1 to 54% (H_2 yield of $\geq 50\%$ was obtained only with a flow rate of ≤ 20 sccm and a H_2O concentration of $\leq 1.5\%$ (mol/mol) [57]). In addition, the energy yield of H_2 (0.25-13 g kWh⁻¹) is also quite low compared with the electrolysis of water (14-20 g kWh⁻¹), which has been commercially and commonly used at small scale and viewed as an expensive route.

The low efficiency of the non-thermal plasmas for water splitting is probably resulted from three aspects: a) a relatively low electron energy of the plasmas that is not high enough for the propagation of the water splitting reaction, which is a strong endothermic reaction ($\Delta G^0=229$ kJ/mol) [58]; b) a fast gas flow that leads to a low residence time; c) the generation of various undesired byproducts such as NH_3 , H_2O_2 , and NO . Therefore, more attempts should be focused on the optimization of the reactor design to obtain a higher electron energy of the plasmas and a longer residence time of water

in the plasmas. In addition, to suppress the production of byproducts, the reaction conditions should be carefully controlled, such as the gas temperature, reactor pressure, as well as the types and concentration of the working gas or added gas. Several authors have demonstrated that, as working gas, Ar could enhance the performance of the water splitting process, with the formation of only a small amount of byproducts (e.g., H₂O₂) [14, 15]. Table 1 also reveals that the addition of O₂ into the plasma system could lead to a decrease in the H₂ yield. In addition, micro-plasma reactors, with a lower power requirement, can better control the water splitting process and are also considered as a promising method to enhance the energy efficiency of plasma water splitting process [10, 59].

Compared to other non-thermal plasma systems, the RGA plasma shows a highest H₂ production rate in plasma water splitting process. It is also interesting to note that the RGA plasmas can provide a relatively high feed flow rate (or processing capacity), while allowing for a wider range of input H₂O concentration. The high H₂ production rate, with a maximum of 41.3 μmols^{-1} that is much higher than that of other plasmas, is resulted from the relatively high energy density of the RGA plasmas with increased retention time of reactant in plasmas due to the rapid rotation of the arc [17]. Whereas, the H₂ energy yields are unsatisfactory, which is probably due to the relatively low electron temperature in the RGA plasmas (approximately 1 eV) [17]. Further works will focus on the minimization and optimization of the reactor to obtain a higher electron temperature and therefore a higher energy efficiency.

Table. 1 Comparison of performance of water splitting by various technologies

Method	Working gas	Power supply and/or discharge power	Input flow rate Q _{gas} (L/min), Q _{H2O} (ml/min)	Input H ₂ O concentration (%(mol/mol))	H ₂ yield (%)	H ₂ production rate (μmols^{-1})	Energy yield of H ₂ (g kWh ⁻¹)	Ref.
Electrolysis	-	-	-	-	-	-	14-20	[60-62]
Photocatalysis	-	-	-	-	-	~0.01	0.01	[63]
Pulsed corona	N ₂	37-72 W	Under water discharge	-	-	~0.4-0.8	~0.25	[11]
DBD	N ₂	AC, 7.8 kV, 50Hz	Q _{gas} : 0.01-1.5	1-2.5	1-29	<0.22	-	[61]
Glow discharge	He	AC, 0.44-1.29 kV, 8.1kHz	Q _{gas} : 0.01-0.08	2.9-3.1	8-54	-	-	[57]
Tubular plasma-catalyst	Ar	AC, 0.28-0.72 kV 8.1 kHz,	Q _{gas} : 0.01	2.3	3.8-14.2	0.006-0.085	-	[64]

Micro-hollow cathode	SO ₂	AC, 0.5-2.0mA, 1-20kHz, 0.15-0.45 W	Q _{gas} : 0.03 or 0.1; Q _{H2O} : 100-500	>99	-	~2.5-5.3	-	[12]
Flat pulsed gliding arc	Ar	25 kV, 250 Hz, 1.5 W	Q _{gas} : 2; Q _{H2O} : 1-20	~38.4-92.6	-	~0.25-0.55	~5-13	[14]
	Air					~0.15-0.32	~4-8	
	N ₂					~0.05-0.10	~1-2	
Flat AC gliding arc	CO ₂	AC, 12 kV, 250 W	Q _{gas} : 2.2 or 3.7; Q _{H2O} : 25	93.4 or 89.4	-	12	-	[15]
	N ₂					17.3		
	O ₂					0.3		
	Ar					20.7		
	He					4.1		
RGA	N ₂	DC, 10kV 123.2-367.5 W	Q _{gas} : 2-14.1; Q _{H2O} : 0.1-2.7	1-30	1.2-12.4	10.4-41.3	0.32-0.96	This work

Conclusions

A detailed study of hydrogen production from water splitting by an RGA plasma has been performed. Results show that the H₂ and O₂ yield both decrease with increasing H₂O concentration or total flow rate, and vary over the range of 1.2-12.4% and 0.8-53.0%, respectively. Due to the formation of NH radicals, NH₃ molecules, and some O-containing byproducts such as H₂O₂, O₃, and NO, the H₂/O₂ ratio vary from 0.47 to 2.9 with increasing H₂O concentration. Compared to other non-thermal plasma systems, the RGA plasma shows a highest H₂ production rate in plasma water splitting process. It is also interesting to note that the RGA plasmas can provide a relatively high feed flow rate (or processing capacity), while allowing for a wider range of input H₂O concentration.

Optical emission diagnostics has shown that NO, OH, NH, N₂, and N₂⁺ are detected in the N₂/H₂O spectra, and the OH and NH spectral lines become more and more predominant with increasing H₂O concentration. OH intensity increases with increasing H₂O concentration. In addition to the direct electron impact dissociation of H₂O, and the dissociative electron recombination of H₂O⁺ (H₃O⁺), the reaction of excited N₂(A) with H₂O molecules is also considered to play an important role in the generation of OH radicals.

The complex reactions in the N₂/H₂O plasma bulk are initiated from the excitation, ionization, and/or dissociation of H₂O and/or N₂ molecules, producing various key intermediate species such as OH, H, H₂O⁺ (H₃O⁺), N₂⁺, N₂(A), and/or N etc., which will then lead to the formation of H₂, O₂, H₂O₂, NO (or NO₂), and NH₃ etc. via coupling reactions among each other.

The rotational temperature of N₂⁺, which can be considered as the gas temperature, shows a

significant drop from 2875 ± 125 to 1725 ± 25 K with the addition of 1% (mol/mol) H_2O into N_2 . Increasing total flow rate from 0.1 to 0.5 mol/min leads to a slight decrease of the rotational temperature of N_2^+ , whereas a further increase of flow rate to 0.7 mol/min results in a significant drop of the rotational temperature from 1600 ± 25 to 1075 ± 75 K.

Acknowledgments

This work is supported by the National Natural Science Foundation of China (51576174), the Specialized Research Fund for the Doctoral Program of Higher Education of China (20120101110099) and the Fundamental Research Funds for the Central Universities (2015FZA4011).

References

- [1]. Simpson AP, Lutz AE (2007) Exergy analysis of hydrogen production via steam methane reforming. *Int J Hydrogen Energy* 32:4811-4820.
- [2]. Šingliar M (2007) Solar energy using for hydrogen production. *Petroleum & Coal* 49:40-47.
- [3]. Fujishima A, Honda K (1972) Electrochemical photolysis of water at a semiconductor electrode. *Nature* 238:37-38.
- [4]. Domen K, Kondo JN, Hara M, Takata T (2000) Photo-and mechano-catalytic overall water splitting reactions to form hydrogen and oxygen on heterogeneous catalysts. *B Chem Soc Jpn* 73:1307-1331.
- [5]. Perkins C, Weimer AW (2004) Likely near-term solar-thermal water splitting technologies. *Int J Hydrogen Energy* 29:1587-1599.
- [6]. Ni M, Leung MK, Leung DY, Sumathy K (2007) A review and recent developments in photocatalytic water-splitting using TiO_2 for hydrogen production. *Renewable Sustainable Energy Rev* 11:401-425.
- [7]. Tu X, Whitehead JC (2014) Plasma dry reforming of methane in an atmospheric pressure AC gliding arc discharge: Co-generation of syngas and carbon nanomaterials. *Int J Hydrogen Energy* 39:9658-9669.
- [8]. Liu SY, Mei DH, Shen Z, Tu X (2014) Nonoxidative conversion of methane in a dielectric barrier discharge reactor: Prediction of reaction performance based on neural network model. *J. Phys. Chem. C* 118:10686-10693.
- [9]. Wang WZ, Murphy AB, Yan JD, Rong MZ, Spencer JW, Fang MTC (2012) Thermophysical properties of high-temperature reacting mixtures of carbon and water in the range 400–30,000 K and 0.1–10 atm. Part 1: equilibrium composition and thermodynamic properties. *Plasma Chem Plasma Process* 32:75-96.
- [10]. Rehman F, Lozano-Parada JH, Zimmerman WB (2012) A kinetic model for H_2 production by plasmolysis of water

vapours at atmospheric pressure in a dielectric barrier discharge microchannel reactor. *Int J Hydrogen Energy* 37:17678-17690.

[11]. Kirkpatrick MJ, Locke BR (2005) Hydrogen, oxygen, and hydrogen peroxide formation in aqueous phase pulsed corona electrical discharge. *Ind Eng Chem Res* 44:4243-4248.

[12]. Koo IG, Choi MY, Kim JH, Cho JH, Lee WM (2008) Microdischarge in porous ceramics with atmospheric pressure high temperature $\text{H}_2\text{O}/\text{SO}_2$ gas mixture and its application for hydrogen production. *Jpn J Appl Phys* 47:4705.

[13]. Kabashima H, Einaga H, Futamura S (2003) Hydrogen generation from water, methane, and methanol with nonthermal plasma. *IEEE Trans Ind Appl* 39:340-345.

[14]. Burlica R, Shih K, Locke BR (2010) Formation of H_2 and H_2O_2 in a water-spray gliding arc nonthermal plasma reactor. *Ind Eng Chem Res* 49:6342-6349.

[15]. Porter D, Poplin MD, Holzer F, Finney WC, Locke BR (2009) Formation of hydrogen peroxide, hydrogen, and oxygen in gliding arc electrical discharge reactors with water spray. *IEEE Trans Ind Appl* 45:623-629.

[16]. Burlica R, Locke BR (2008) Pulsed plasma gliding-arc discharges with water spray. *IEEE Trans Ind Appl* 44:482-489.

[17]. Zhang H, Du CM, Wu AJ, Bo Z, Yan JH, Li XD (2014) Rotating gliding arc assisted methane decomposition in nitrogen for hydrogen production. *Int J Hydrogen Energy* 39:12620-12635.

[18]. Cormier JM, Dudemaine M, Rusu I (2002) On a new magnetic blow out glidarc reactor. In: 8th International symposium on high pressure, low temperature plasma chemistry, Pühajärve, pp 176-180.

[19]. Cormier JM, Rusu I, Khacef A (2003) On the use of a magnetic blow out glidarc reactor for the syngas production by steam reforming. In: 16th International symposium on plasma chemistry, Toarmina.

[20]. Hnatiuc E, Burlui V, Ursache M, Astanei D, Hnatiuc B (2012) About the operation of the cold plasma GlidArc type reactors with rotary discharge and auxiliary electrodes. In: 13th International conference on optimization of electrical and electronic equipment, Brasov, pp 1353-1358.

[21]. Lee DH, Kim K, Cha MS, Song Y (2007) Optimization scheme of a rotating gliding arc reactor for partial oxidation of methane. *P Combust Inst* 31:3343-3351.

[22]. Zhang H, Li XD, Zhang YQ, Chen T, Yan JH, Du CM (2012) Rotating gliding arc codriven by magnetic field and tangential flow. *IEEE Trans Plasma Sci* 40:3493-3498.

[23]. Zhang H, Li XD, Zhu FS, Bo Z, Cen KF, Tu X (2015) Non-oxidative decomposition of methanol into hydrogen in a rotating gliding arc plasma reactor. *Int J Hydrogen Energy* 40:15901-15912.

[24]. Park JY, Kostyuk PV, Han SB, Kim JS, Vu CN, Lee HW (2006) Study on optical emission analysis of AC

air–water discharges under He, Ar and N₂ environments. *J Phys D: Appl Phys* 39:3805.

[25]. Zhang H, Zhu FS, Bo Z, Cen KF, Li XD (2015) Hydrogen production from methanol decomposition in a gliding arc discharge plasma with high processing capacity. *Chem Lett* 44:1315-1317.

[26]. Legrand JC, Damiy AM, Hrach R, Hrachova V (1997) Methane conversion in the flowing afterglow of a dinitrogen microwave plasma: Initiation of the reaction. *Contrib Plasm Phys* 37:521-537.

[27]. Aerts R, Tu X, De Bie C, Whitehead JC, Bogaerts A (2012) An investigation into the dominant reactions for ethylene destruction in non-thermal atmospheric plasmas. *Plasma Processes Polym* 9:994-1000.

[28]. Panousis E, Merbahi N, Clement F, Ricard A, Yousfi M, Papageorghiou L, Loiseau JF, Eichwald O, Held B, Spyrou N (2009) Atmospheric pressure dielectric barrier discharges under unipolar and bipolar HV excitation in view of chemical reactivity in afterglow conditions. *IEEE Tran Plasma Sci* 37:1004-1015.

[29]. Simek M, Babický V, Clupek M, DeBenedictis S, Dilecce G, Sunka P (1998) Excitation of N₂(C) and NO(A) states in a pulsed positive corona discharge in -O₂ and -NO mixtures. *J Phys D: Appl Phys* 31:2591.

[30]. Verreycken T, Bruggeman PJ (2014) OH density measurements in nanosecond pulsed discharges in atmospheric pressure N₂-H₂O mixtures. *Plasma Sources Sci Technol* 23:15009.

[31]. Ono R, Oda T (2001) OH radical measurement in a pulsed arc discharge plasma observed by a LIF method. *IEEE Trans Ind Appl* 37:709-714.

[32]. Srivastava N, Wang C (2011) Effects of water addition on OH radical generation and plasma properties in an atmospheric argon microwave plasma jet. *J Appl Phys* 110:053304.

[33]. Sun M, Wu Y, Li J, Wang NH, Wu J, Shang KF, Zhang JL (2005) Diagnosis of OH radical by optical emission spectroscopy in atmospheric pressure unsaturated humid air corona discharge and its implication to desulphurization of flue gas. *Plasma Chem Plasma Process* 25:31-40.

[34]. Bruggeman P, Iza F, Guns P, Lauwers D, Kong MG, Gonzalvo YA, Leys C, Schram DC (2010) Electronic quenching of OH (A) by water in atmospheric pressure plasmas and its influence on the gas temperature determination by OH (A-X) emission. *Plasma Sources Sci Technol* 19:15016.

[35]. Bruggeman P, Schram DC, Kong MG, Leys C (2009) Is the rotational temperature of OH (A-X) for discharges in and in contact with liquids a good diagnostic for determining the gas Temperature? *Plasma Processes Polym* 6:751-762.

[36]. Bruggeman P, Schram D, Gonzalez MA, Rego R, Kong MG, Leys C (2009) Characterization of a direct dc-excited discharge in water by optical emission spectroscopy. *Plasma Sources Sci Technol* 18:25017.

[37]. Pintassilgo CD, Loureiro J (2009) Production of hydrocarbons and nitriles using a N₂-CH₄ afterglow plasma for simulation of Titan's atmosphere. *Planet Space Sci* 57:1621-1630.

- [38]. Pintassilgo CD, Loureiro J (2010) Kinetic study of a $\text{N}_2\text{-CH}_4$ afterglow plasma for production of N-containing hydrocarbon species of Titan's atmosphere. *Adv Space Res* 46:657-671.
- [39]. Liu F, Wang W, Zheng W, Wang Y (2006) Optical study of radicals (OH, O, H, N) in a needle-plate bi-directional pulsed corona discharge. *Eur Phys J D* 38:515-522.
- [40]. Eichwald O, Yousfi M, Hennad A, Benabdessadok MD (1997) Coupling of chemical kinetics, gas dynamics, and charged particle kinetics models for the analysis of NO reduction from flue gases. *J Appl Phys* 82:4781-4794.
- [41]. Hagelaar GJM, Pitchford LC (2005) Solving the Boltzmann equation to obtain electron transport coefficients and rate coefficients for fluid models. *Plasma Sources Sci Technol* 14:722.
- [42]. Damiy A, Hrach R, Hrachova V, Legrand J (2001) Influence of C atom concentration for acetylene production in a CH_4/N_2 afterglow. *Vacuum* 61:403-407.
- [43]. Tu X, Yu L, Yan JH, Cen KF, Chéron BG (2009) Dynamic and spectroscopic characteristics of atmospheric gliding arc in gas-liquid two-phase flow. *Phys Plasmas* 16: 113506.
- [44]. Van Helden JH, van den Oever PJ, Kessels W, Van de Sanden M, Schram DC, Engeln R (2007) Production mechanisms of NH and NH_2 radicals in $\text{N}_2\text{-H}_2$ plasmas. *J Phys Chem A* 111:11460-11472.
- [45]. Wang C, Wu W (2013) Simultaneous measurements of OH(A) and OH(X) radicals in microwave plasma jet-assisted combustion of methane/air mixtures around the lean-burn limit using optical emission spectroscopy and cavity ringdown spectroscopy. *J Phys D: Appl Phys* 46:464008.
- [46]. Jauberteau JL, Jauberteau I, Aubreton J (2002) NH_3 and $\text{NH}_{x<3}$ radicals synthesis downstream a microwave discharge sustained in an $\text{Ar-N}_2\text{-H}_2$ gas mixture. Study of surface reactive processes and determination of rate constants. *J Phys D: Appl Phys* 35:665.
- [47]. Burlica R, Kirkpatrick MJ, Locke BR (2006) Formation of reactive species in gliding arc discharges with liquid water. *J Electrostat* 64:35-43.
- [48]. Burlica R, Hnatiuc B, Hnatiuc E (2010) Hydrogen and hydrogen peroxide formation in the AC water-spray gliding arc reactor. In *IEEE 12th International Conference on Optimization of Electrical and Electronic Equipment (OPTIM)*: 1355-1360.
- [49]. Dorier JL, Gindrat M, Hollenstein C, Salito A, Loch M, Barbezat G (2001) Time-resolved imaging of anodic arc root behavior during fluctuations of a DC plasma spraying torch. *IEEE Trans Plasma Sci* 29:494-501.
- [50]. Sarani A, Nikiforov AY, Leys C (2010) Atmospheric pressure plasma jet in Ar and $\text{Ar/H}_2\text{O}$ mixtures: Optical emission spectroscopy and temperature measurements. *Phys Plasmas* 17:63504.
- [51]. Zhang H, Zhu FS, Tu X, Bo Z, Cen KF, Li XD (2015) Characteristics of atmospheric pressure rotating gliding arc

plasmas. Plasma Sci Technol (In press).

[52]. Luque J, Crosley DR (1999) LIFBASE: Database and spectral simulation (version 1.5). SRI International report MP: 99-009.

[53]. Moon SY, Choe W (2003) A comparative study of rotational temperatures using diatomic OH, O₂ and N₂⁺ molecular spectra emitted from atmospheric plasmas. Spectrochim Acta, Part B 58:249-257.

[54]. Ono R, Teramoto Y, Oda T (2010) Effect of humidity on gas temperature in the afterglow of pulsed positive corona discharge. Plasma Sources Sci Technol 19:15009.

[55]. Czernichowski A, Nassar H, Ranaivosoloarimanana A, Fridman AA, Simek M, Musiol K, Pawelec E, Dittrichova L (1996) Spectral and electrical diagnostics of gliding arc. Acta Phys Pol, A 89:595-604.

[56]. Zhao T, Xu Y, Song Y, Li X, Liu J, Liu J, Zhu A (2013) Determination of vibrational and rotational temperatures in a gliding arc discharge by using overlapped molecular emission spectra. J Phys D: Appl Phys 46:345201.

[57]. Suib SL, Brock SL, Marquez M, Luo J, Matsumoto H, Hayashi Y (1998) Efficient catalytic plasma activation of CO₂, NO, and H₂O. J. Phys. Chem. B 102:9661-9666.

[58]. Luo J, Suib S, Hayashi Y, Matsumoto H (2000) Water splitting in low-temperature ac plasmas at atmospheric pressure. Res Chem Intermed 26:849-874.

[59]. Lozano-Parada JH, Zimmerman WB (2010) The role of kinetics in the design of plasma microreactors. Chem Eng Sci 65:4925-4930.

[60]. Holladay JD, Hu J, King DL, Wang Y (2009) An overview of hydrogen production technologies. Catal Today 139:244-260.

[61]. Kabashima H, Einaga H, Futamura S (2001) Hydrogen generation from water with nonthermal plasma. Chem Lett 12:1314-1315.

[62]. Turner J, Sverdrup G, Mann MK, Maness PC, Kroposki B, Ghirardi M, Evans RJ, Blake D (2008) Renewable hydrogen production. Int J Energ Res 32:379-407.

[63]. Kudo A. Development of photocatalyst materials for water splitting (2006) Int J Hydrogen Energy 31:197-202.

[64]. Chen X, Suib SL, Hayashi Y, Matsumoto H (2001) H₂O splitting in tubular PACT (Plasma and catalyst integrated technologies) reactors. J Catal 201:198-205